

## Synthesis-Dependent Atomic Surface Structures of Oxide Nanoparticles

Yuyuan Lin,<sup>1,\*</sup> Jianguo Wen,<sup>2</sup> Linhua Hu,<sup>3</sup> Robert M. Kennedy,<sup>3</sup> Peter C. Stair,<sup>3,4</sup>  
Kenneth R. Poeppelmeier,<sup>3,4</sup> and Laurence D. Marks<sup>1,†</sup>

<sup>1</sup>*Department of Materials Science and Engineering, Northwestern University, Evanston, Illinois 60208, USA*

<sup>2</sup>*Electron Microscopy Center, Argonne National Laboratory, Argonne, Illinois 60439, USA*

<sup>3</sup>*Department of Chemistry, Northwestern University, Evanston, Illinois 60208, USA*

<sup>4</sup>*Chemical Sciences and Engineering Division, Argonne National Laboratory, Argonne, Illinois 60439, USA*

(Received 10 May 2013; published 8 October 2013)

Using SrTiO<sub>3</sub> nanocuboids as a model system, we show with aberration-corrected high resolution electron microscopy at sub-Å resolution that surface relaxations or reconstructions are present on the nanocuboids, depending on the synthetic process. Oleic acid synthesis, acetic acid synthesis, and microwave-assisted acetic acid synthesis result in a SrO termination, TiO<sub>2</sub>-rich reconstruction, and mixed termination, respectively. The experimental atomic positions are in better agreement with density functional theory calculations using an exact-exchange corrected PBEsol functional than the Perdew-Burke-Ernzerhof (PBE) functional.

DOI: [10.1103/PhysRevLett.111.156101](https://doi.org/10.1103/PhysRevLett.111.156101)

PACS numbers: 68.37.Og, 68.35.B-, 68.35.Md

The surface of SrTiO<sub>3</sub> is one of the most studied because of its importance for applications ranging from thin film substrates [1,2] to catalytic supports [3], and in photocatalysis [4]. Similar to the surface of other oxides (e.g., [5–7]), a variety of reconstructions on SrTiO<sub>3</sub> single crystals have been observed. For example, the (2 × 1) [8–10], (2 × 2) [11–13], *c*(4 × 2) [8,14–16], *c*(4 × 4) [8,13], (6 × 2) [17], and many more [18] are known to exist. A simple but harsh question often asked in the surface science community is whether these reconstructions are relevant in real applications. Herein, we use aberration-corrected high resolution electron microscopy (HREM) profile-view imaging demonstrating that different surface structures are present on SrTiO<sub>3</sub> nanocuboids, dependent on the synthesis method.

The SrTiO<sub>3</sub> nanocuboids used have a well-defined, thermodynamically stable shape with primarily (100) type surfaces exposed. In single crystal studies, the well-ordered (2 × 1), (2 × 2), *c*(4 × 2) reconstructions, all of which were found to contain TiO<sub>2</sub> double layers (a surface excess of 1.5 TiO<sub>2</sub>/1 × 1 surface cell), have been structurally solved for the SrTiO<sub>3</sub> (100) surface [9,15,19–21]. More recently, glasslike locally ordered structures of ( $\sqrt{13} \times \sqrt{13}$ )R33.7° (RT13), (3 × 3), and ( $\sqrt{5} \times \sqrt{5}$ )R26.6° (RT5) were solved and found to be stable for lower surface excesses of TiO<sub>2</sub> [22]. All these reconstructions have been observed for samples prepared with an ion-beam cleaning or thinning step which leads to a TiO<sub>2</sub>-rich surface; in principle, other surface structures such as a SrO termination can occur if the surface composition is changed.

Three methods of synthesizing the SrTiO<sub>3</sub> nanocuboids were employed. The first was a hydrothermal process within a lamellar microemulsion involving oleic acid which also acts as a surfactant [23], the second was a hydrothermal process without an ordered microemulsion

using acetic acid [24], the third was the same type of synthesis as the second one but the hydrothermal process was conducted in a microwave oven. The average sizes for the nanocuboids from the three syntheses are approximately 20, 65, and 35 nm, respectively. We will refer to the three syntheses as oleic acid, acetic acid, and MA-HT syntheses later. The HREM experiments were performed using a FEI Titan 80–300 TEM operated at 200 keV with spherical (Cs) and chromatic (Cc) aberration correctors [25]. The as-prepared SrTiO<sub>3</sub> nanocuboids were mixed with ethanol and deposited on a lacey carbon film supported on a copper grid. The Cc was tuned to be less than 1 μm and the Cs corrected to close to 0 μm. The other aberrations of the objective lens were tuned to an acceptable level on an amorphous area before image recording. After the sample was tilted to a (110) zone axis, a through-focal series of images were taken of the same area with 2 nm steps.

Density functional theory (DFT) calculations were performed with the all-electron augmented plane wave + local orbitals WIEN2K code [26]. The surface in-plane lattice parameters were set to those for the corresponding DFT optimized bulk cell, and a *N* × *N* × 10 supercell for a *N* × *N* surface reconstruction was used with ~1.6 nm of vacuum to avoid errors within the DFT calculations as well as in the image simulations. Muffin-tin radii were set to 1.6, 2.45, and 1.8 Bohr for O, Sr, and Ti, respectively, as well as a min(RMT)*K*<sub>max</sub> of 7.5 and a 16/*N* × 16/*N* × 1 *k*-point grid. For the surface reconstructions, the models were obtained directly from previous studies [9,15,22,27], relaxed as needed (see Supplemental Material [28] for atomic positions). In addition to conventional DFT calculations with the Perdew-Burke-Ernzerhof (PBE) functional [29] we also used an on-site hybrid [30,31] PBEsol0 functional which is based upon the PBEsol functional [32] with

some fraction of exact exchange for the Ti  $d$  electrons. The onsite exact exchange fraction 0.5 was previously determined as the best fit to the energetics of a range of  $\text{TiO}_x$  clusters and bulk thermodynamics [33].

The simulation of the HREM images was performed using the MacTempas program based on the multislice method [34] and conventional nonlinear imaging theory [35]. The DFT relaxed structures were rescaled to the bulk lattice parameters (for PBE this was a 0.32% contraction, for PBEsol0 a 0.18% expansion). Detailed simulation procedures are described in the Supplemental Material [28]. While the samples have locally varying thicknesses, due to their geometry this is known *a priori* so relevant thicknesses were used without any adjustable parameters (no Stobbs factor) with images for different thicknesses spliced together which is a good approximation due to zone-axis channeling. The peak positions for both the experimental and simulated images were measured by fitting the intensity maxima with two dimensional single Gaussian functions.

A typical  $\text{SrTiO}_3$  nanocuboid synthesized by the oleic acid method imaged along the [110] direction is shown in Fig. 1(b). A higher magnification image of this nanocuboid with the surface layer (the top layer) clearly resolved is shown in Fig. 1(a). The contrast in the bulk region can be directly interpreted: the bright spots are atoms. This is consistent with previous HREM study of  $\text{SrTiO}_3$  single crystals under similar imaging conditions (small Cs and small overfocus) [36]. Figure 1(d) shows a simulated HREM image from a DFT relaxed  $\text{SrO}$  ( $1 \times 1$ ) surface, which matches the experimental image. Note that other surface structures can show the same surface periodicity, but the contrast is drastically different from the experimental image (see Supplemental Material [28]). The surface of the nanocuboids synthesized by the oleic acid method has a  $1 \times 1$   $\text{SrO}$  termination.

A detailed measurement of the interlayer spacing in the HREM image based on the Gaussian fitted positions is shown in Fig. 2(a). The spacing of the two outmost surface layers is significantly different from the bulk. For a better comparison, we simulated HREM images using unrelaxed and DFT relaxed surface structures. The interlayer spacing measurement was also conducted on the simulated HREM images, as shown in Fig. 2(a). The results from the DFT relaxed structures match the experiment much better than the unrelaxed structure. The DFT calculations indicate an approximately 13% normal contraction of the outmost layer (d1) and a 5% expansion of the subsurface layer (d2) compared to the bulk. The experimental oscillation of the interlayer spacing in the bulk region is due to residual astigmatism and sample tilt (see Supplemental Material [28]). A careful check of the absolute peak positions shows that the result from the PBEsol0 functional is closer to the experimental results, as shown in Fig. 2(b). With the PBE functional the atomic spacings at the surface

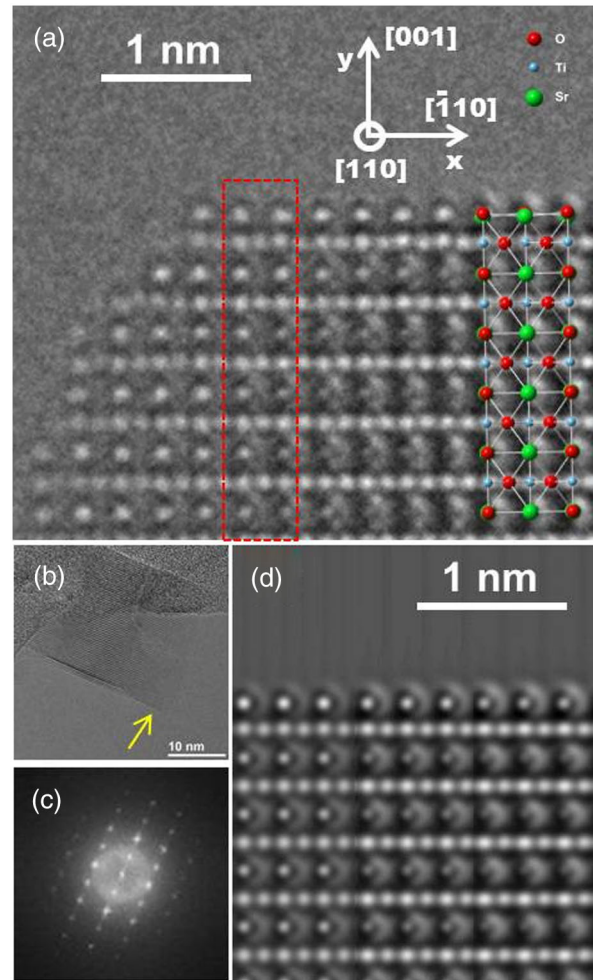


FIG. 1 (color online). HREM study of samples from the oleic acid synthesis. (a) Experimental HREM image of  $\text{SrTiO}_3$  nanocuboid along [110], where the bright spots can be interpreted as atoms. (b) Low magnification image of (a). (c) FFT image of (b). (d) Simulated HREM image of (a). In (a) the sample thickness and defocus are increasing from left to right. Therefore, (d) is generated using 3 images simulated with continual changing defocus and thickness, increasing from left to right.

are contracted too much; this can be understood as the PBE functional is too covalent and overbonds the surface atoms while the hybrid functional overcomes this shortcoming somewhat by correcting the exchange term for the strongly correlated  $d$  electrons of Ti.

The surface of the nanocuboids synthesized by the acetic acid method is shown in Fig. 3(a), in which the bright spots are atoms. To identify the surface structure of the nanocuboids, all the solved surface reconstructions were used to simulate HREM images (see Supplemental Material [28]). The well-ordered  $c(4 \times 2)$ ,  $(2 \times 1)$ , and  $(2 \times 2)$  surface reconstructions can be ruled out, as they all result in localized strong intensity at the surface Ti columns while the intensity for the oxygen columns is too weak and diffuse. The simulated HREM images from the glasslike locally ordered  $RT13$ ,  $(3 \times 3)$  and  $RT5$  surface

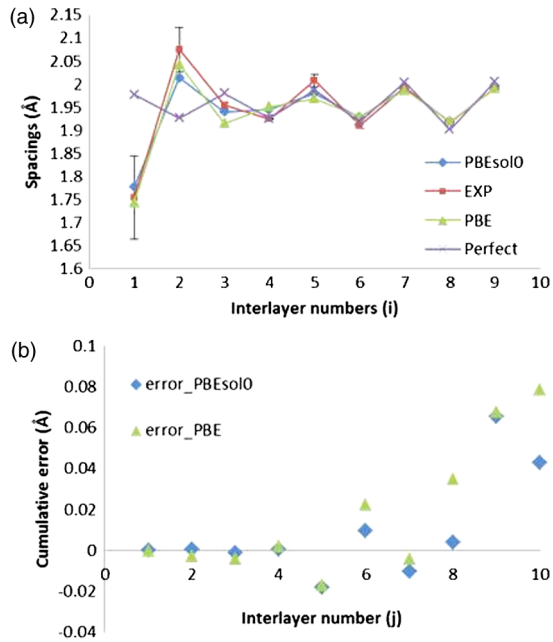


FIG. 2 (color online). (a) Interlayer spacing comparison of the experimental image and simulated images for unrelaxed and DFT relaxed structures. The comparison is based on the area marked in the red box in Fig. 1(a). The interlayer spacings ( $i$ ) are measured from Gaussian fits to the peak positions of the SrO-Ti atomic columns from the surface into the bulk. The error bars indicate the experimental deviation with respect to the mean values. (b) Cumulative error comparison between the DFT calculation using the PBE and the PBEsol0 functional. The base line was chosen as the 10th layer in the bulk from the surface ( $j = 1$  is the 10th interlayer spacing from the surface).

reconstructions match the experimental data much better (see Supplemental Material [28]). A careful investigation of the surface column positions and the intensity profiles shows that RT13 and RT5 surfaces agree slightly better with the experiments than the  $(3 \times 3)$ . There exist models for SrTiO<sub>3</sub> (001) surfaces such as a  $(\sqrt{5} \times \sqrt{5})R26.6^\circ$  containing Sr adatoms [37,38], although DFT calculations have indicated that these require conditions far from equilibrium [39] and are contradicted by more recent, higher-resolution STM images [40]. We also did HREM simulations for this structure and found that the contrast at the surface does not match the experimental images (see Supplemental Material [28]). The simulated image from the RT13 surface with varying thicknesses and defoci is shown in Fig. 3(d). We note that the energy difference between the locally ordered structures is small (see [22] and Supplemental Material [28]), so it is probable that the surface is a combination of the three structures, i.e., a glass. We conclude that the surface termination for this synthesis is a locally ordered TiO<sub>2</sub> glass on top of the  $(1 \times 1)$  TiO<sub>2</sub> subsurface, as predicted [22]. The TiO<sub>2</sub>-rich surface is also consistent with the epitaxy of Pt on acetic acid synthesized SrTiO<sub>3</sub> nanocuboids, which shows a clear cube-on-cube epitaxy [41].

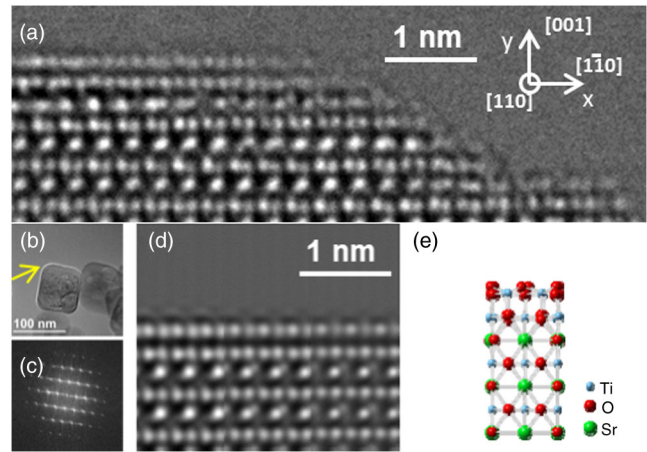


FIG. 3 (color online). HREM images from the acetic acid synthesis. (a) Experimental HREM image of a SrTiO<sub>3</sub> nanocuboid along [110]. (b) Low magnification image of (a). (c) The FFT image of (a). (d) A simulated image using a RT13 reconstructed surface. (e) Illustration of the RT13 atomic surface structures along the [110] viewing direction. In (a), owing to the nature of the sample, the sample thickness and defocus are increasing from right to left. Therefore, (d) was generated using 3 images simulated with different defocus and thickness, increasing from right to left.

The MA-HT synthesis result is shown in Fig. 4(a). For region type I (indicated by the red arrows), the surface can be interpreted as a SrO termination comparable to the oleic acid synthesis case. The simulated HREM image using a SrO terminated surface is shown in Fig. 4(d), which matches with the experimental image well. In contrast, for region type II (indicated by the blue arrows), a reconstruction exists. Using the same methodology as for the previous two syntheses, we found that a locally ordered surface with both TiO<sub>2</sub> double-layer and SrO terminations overlapping along the beam direction matches best with the experimental image in these areas (see Supplemental Material [28]). A simulated HREM for a layered structural model with equal contribution of SrO termination and the  $(3 \times 3)$  reconstructed termination is shown in Fig. 4(d) and shows reasonably good agreement with the experimental images.

It is clear that the surface structure depends upon how the nanocuboids are synthesized. Oleic acid is a typical surfactant, and has a long carbon chain (18 carbons) with separated hydrophobic and hydrophilic groups. As a result, ordered liquid crystal-like structures are formed during the hydrothermal process [23]. With oleic acid, the end product is a nanocuboid coated with a monolayer of relatively strongly bound carboxylate groups, as evidenced from other TEM and FT-IR data (see Supplemental Material [28]). A SrO termination is more basic than a TiO<sub>2</sub> termination [42,43]; hence, the bonding between the Sr cation and oleate anion is energetically favored. As a result, there is a strong driving force for a SrO termination. Note that

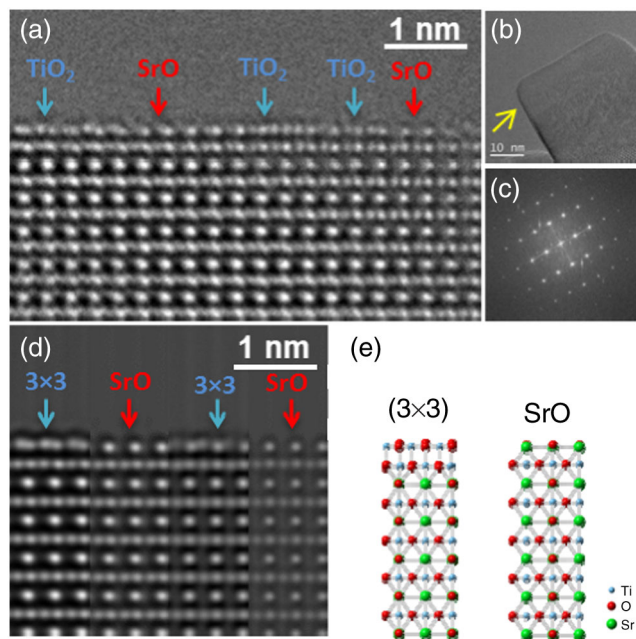


FIG. 4 (color online). HREM images from the MA-HT synthesis. (a) Experimental HREM image of a  $\text{SrTiO}_3$  nanocuboid along  $[110]$ . (b) Low magnification image of (a). (c) The FFT image of (b). (d) A simulated image using a SrO terminated surface (areas with red arrows) and a layered structure model consisting of 50% of SrO and 50% of  $(3 \times 3)$  surface terminations (areas with blue arrows). (e) Illustration of the  $(3 \times 3)$  and SrO atomic surface structures along  $[110]$ . In (a), owing to the nature of the sample, the sample thickness, and defocus are increasing from right to left. Therefore, (d) was generated using 4 images simulated with different defocus and thickness, increasing from right to left.

our HREM samples were washed in ethanol, which can remove the organic ligands on the surface (see Supplemental Material [28]). Thus the surface is sharp and clean in the HREM images.

In contrast, acetic acid is soluble in water and no micro-emulsion structures are present during the hydrothermal process. Energetically the formation of the glasslike locally ordered reconstructions is favored, as they are located on the convex hull [22]. Unlike some reconstructions formed in UHV, the reconstructions of  $\text{SrTiO}_3$  are formed in solution, and they are fully oxidized. While it is possible that there is some absorption on the surface, the absorption is rather weak and does not play an important role on the surface structures. DFT calculations show that for a wet surface of  $\text{SrTiO}_3$  (001), the stable surface structure is the pure reconstructed  $\text{SrTiO}_3$  surface with water molecules rather weakly chemisorbed [44]. In the high vacuum environment of the TEM chamber, as well as the electron beam irradiation, the weakly absorbed molecules desorb quickly and leave the surface of the nanocuboids sharp and atomically flat.

Microwave assisted hydrothermal synthesis is a new technique whose complete role in synthesis is still

unclear [45]. Microwave irradiation can induce different morphologies and even new phases. For example, it was found that for the synthesis of  $\text{BaTiO}_3$  nanoparticles, the particle size, phase purity, and surface areas are influenced by the microwave frequency [46], and microwave irradiation on the as-prepared truncated  $\text{BaTiO}_3$  nanocubes can enhance a ferroelectric phase transformation [47]. It is clear that the electric field couples with the dielectric constant of the precursors and the end products. Exactly why microwave irradiation enhances the SrO termination and makes the surface more stoichiometric (similar amount of surface SrO and  $\text{TiO}_2$ ), we leave as an open question for future study.

It is worth noting that the commonly assumed  $(1 \times 1)$   $\text{TiO}_2$  surface termination does not exist for any of the syntheses. This is expected as the surface energy of  $(1 \times 1)$   $\text{TiO}_2$  termination is above the convex hull.

In summary, we have shown that for  $\text{SrTiO}_3$  nanoparticles the atomic surface structures are synthesis dependent. The SrO termination and the locally ordered  $\text{TiO}_2$ -rich surface reconstructions are in agreement with surface acidity as well as DFT energetics. The microwave irradiation results in a more stoichiometric mixed surface termination. These findings are of relevance for catalytic and thin film applications where  $\text{SrTiO}_3$  is a popular substrate, and should be qualitatively extendable to other oxide nanoparticles.

We acknowledge funding from Northwestern University Institute for Catalysis in Energy Processes (ICEP) on Grant No. DOE DE-FG02-03-ER15457 (Y.L., L.H., P.C.S., K.R.P., and L.D.M.). The electron microscopy was performed at the Electron Microscopy Center for Materials Research at Argonne National Laboratory, a U.S. Department of Energy Office of Science Laboratory operated under Contract No. DE-AC02-06CH11357 by UChicago Argonne, LLC. R.K.'s work is based upon work supported as part of the Institute for Atom-Efficient Chemical Transformations (IACT), an Energy Frontier Research Center funded by the U.S. Department of Energy, Office of Science, Office of Basic Energy Sciences.

\*YuyuanLin2014@u.northwestern.edu

†l-marks@northwestern.edu

- [1] A. Ohtomo, D. A. Muller, J.L. Grazul, and H. Y. Hwang, *Nature (London)* **419**, 378 (2002).
- [2] A. Ohtomo and H. Y. Hwang, *Nature (London)* **427**, 423 (2004).
- [3] J. A. Enterkin, W. Setthapun, J.W. Elam, S.T. Christensen, F.A. Rabuffetti, L.D. Marks, P.C. Stair, K.R. Poeppelmeier, and C.L. Marshall, *ACS Catal.* **1**, 629 (2011).
- [4] J.G. Mavroides, J.A. Kafalas, and D.F. Kolesar, *Appl. Phys. Lett.* **28**, 241 (1976).
- [5] U. Diebold, *Surf. Sci. Rep.* **48**, 53 (2003).

- [6] M. Batzill and U. Diebold, *Prog. Surf. Sci.* **79**, 47 (2005).
- [7] A. M. Kolpak, D. Li, R. Shao, A. M. Rappe, and D. A. Bonnell, *Phys. Rev. Lett.* **101**, 036102 (2008).
- [8] M. R. Castell, *Surf. Sci.* **505**, 1 (2002).
- [9] N. Erdman, K. R. Poeppelmeier, M. Asta, O. Warschkow, D. E. Ellis, and L. D. Marks, *Nature (London)* **419**, 55 (2002).
- [10] K. Johnston, M. R. Castell, A. T. Paxton, and M. W. Finnis, *Phys. Rev. B* **70**, 085415 (2004).
- [11] B. Cord and R. Courths, *Surf. Sci.* **162**, 34 (1985).
- [12] F. Silly and M. R. Castell, *Appl. Phys. Lett.* **87**, 053106 (2005).
- [13] F. Silly, D. T. Newell, and M. R. Castell, *Surf. Sci.* **600**, 219 (2006).
- [14] Q. D. Jiang and J. Zegenhagen, *Surf. Sci.* **425**, 343 (1999).
- [15] N. Erdman, O. Warschkow, M. Asta, K. R. Poeppelmeier, D. E. Ellis, and L. D. Marks, *J. Am. Chem. Soc.* **125**, 10050 (2003).
- [16] G.-z. Zhu, G. Radtke, and G. A. Botton, *Nature (London)* **490**, 384 (2012).
- [17] M. R. Castell, *Surf. Sci.* **516**, 33 (2002).
- [18] D. T. Newell, Ph.D. thesis, University of Cambridge, 2007.
- [19] O. Warschkow, M. Asta, N. Erdman, K. R. Poeppelmeier, D. E. Ellis, and L. D. Marks, *Surf. Sci.* **573**, 446 (2004).
- [20] R. Heger, P. R. Willmott, O. Bunk, C. M. Schlepütz, B. D. Patterson, and B. Delley, *Phys. Rev. Lett.* **98**, 076102 (2007).
- [21] C. H. Lanier, A. van de Walle, N. Erdman, E. Landree, O. Warschkow, A. Kazimirov, K. R. Poeppelmeier, J. Zegenhagen, M. Asta, and L. D. Marks, *Phys. Rev. B* **76**, 045421 (2007).
- [22] D. M. Kienzle, A. E. Becerra-Toledo, and L. D. Marks, *Phys. Rev. Lett.* **106**, 176102 (2011).
- [23] L. Hu, C. Wang, S. Lee, R. E. Winans, L. D. Marks, and K. R. Poeppelmeier, *Chem. Mater.* **25**, 378 (2013).
- [24] F. A. Rabuffetti, H.-S. Kim, J. A. Enterkin, Y. Wang, C. H. Lanier, L. D. Marks, K. R. Poeppelmeier, and P. C. Stair, *Chem. Mater.* **20**, 5628 (2008).
- [25] B. Kabius, P. Hartel, M. Haider, H. Muller, S. Uhlemann, U. Loebau, J. Zach, and H. Rose, *J. Electron Microsc.* **58**, 147 (2009).
- [26] P. Blaha *et al.* (Technical University Vienna, 2001).
- [27] Y. Lin, A. E. Becerra-Toledo, F. Silly, K. R. Poeppelmeier, M. R. Castell, and L. D. Marks, *Surf. Sci.* **605**, L51 (2011).
- [28] See Supplemental Material at <http://link.aps.org/supplemental/10.1103/PhysRevLett.111.156101> for detailed HREM multislice simulations, evidence for SrTiO<sub>3</sub> nanocuboids covered by oleate layer, convex hull and DFT relaxed SrO terminated surface structures
- [29] J. P. Perdew, K. Burke, and M. Ernzerhof, *Phys. Rev. Lett.* **77**, 3865 (1996).
- [30] P. Novák, J. Kuneš, L. Chaput, and W. E. Pickett, *Phys. Status Solidi B* **243**, 563 (2006).
- [31] F. Tran, P. Blaha, K. Schwarz, and P. Novák, *Phys. Rev. B* **74**, 155108 (2006).
- [32] J. Perdew, A. Ruzsinszky, G. Csonka, O. Vydrov, G. Scuseria, L. Constantin, X. Zhou, and K. Burke, *Phys. Rev. Lett.* **100**, 136406 (2008).
- [33] L. D. Marks, A. N. Chiamonti, F. Tran, and P. Blaha, *Surf. Sci.* **603**, 2179 (2009).
- [34] J. M. Cowley and A. F. Moodie, *Acta Crystallogr.* **10**, 609 (1957).
- [35] M. A. O'Keefe, in *Proceedings of the 37th Annual Meeting of the Electron Microscopy Society of America, San Antonio, Texas, 1979*, edited by G. W. Bailey (Claitor's Publishing Division, Baton Rouge, 1979), p. 556.
- [36] C. L. Jia, M. Lentzen, and K. Urban, *Science* **299**, 870 (2003).
- [37] T. Kubo and H. Nozoye, *Phys. Rev. Lett.* **86**, 1801 (2001).
- [38] D. T. Newell, A. Harrison, F. Silly, and M. R. Castell, *Phys. Rev. B* **75**, 205429 (2007).
- [39] L. M. Liborio, C. G. Sánchez, A. T. Paxton, and M. W. Finnis, *J. Phys. Condens. Matter* **17**, L223 (2005).
- [40] I. Shiraki and K. Miki, *Surf. Sci.* **605**, 1304 (2011).
- [41] J. A. Enterkin, K. R. Poeppelmeier, and L. D. Marks, *Nano Lett.* **11**, 993 (2011).
- [42] F. A. Rabuffetti, P. C. Stair, and K. R. Poeppelmeier, *J. Phys. Chem. C* **114**, 11056 (2010).
- [43] J. Poth, R. Haberkorn, and H. P. Beck, *J. Eur. Ceram. Soc.* **20**, 715 (2000).
- [44] A. E. Becerra-Toledo, J. A. Enterkin, D. M. Kienzle, and L. D. Marks, *Surf. Sci.* **606**, 791 (2012).
- [45] X. H. Zhu and Q. M. Hang, *Micron* **44**, 21 (2013).
- [46] E. K. Nyutu, C.-H. Chen, P. K. Dutta, and S. L. Suib, *J. Phys. Chem. C* **112**, 9659 (2008).
- [47] V. Swaminathan, S. S. Pramana, T. J. White, L. Chen, R. Chukka, and R. V. Ramanujan, *ACS Appl. Mater. Interfaces* **2**, 3037 (2010).